

IAC-21,C1,1,6,x65166

Combined control and navigation approach to the robotic capture of space vehicles

Zeno Pavanello^{a*}, Francesco Branz^a, Alessandro Francesconi^a, Angelo Cenedese^a, Riccardo Antonello^a, Federico Basana^a, Pietro Iob^a, Davide Vertuani^a, Mauro Massari^b, Camilla Colombo^b, Marco Lovera^b, Davide Invernizzi^b, Pietro Ghignoni^b, Lorenzo Ticozzi^b, Giacomo Borelli^b, Roberto Opromolla^c, Michele Grassi^c, Giancarmine Fasano^c, Alessia Nocerino^c, Carlo Lombardi^c, Claudio Vela^c, Irene Huertas Garcia^d, Pedro Simplicio^d

^aCentre of Studies and Activities for Space “Giuseppe Colombo” (CISAS), Univ. degli Studi di Padova, Padua, Italy

^bDip. di Scienze e Tecnologie Aerospaziali, Politecnico di Milano, Milan, Italy

^cDip. di Ingegneria Industriale, Univ. degli Studi di Napoli “Federico II”, Napoli, Italy

^dESTEC, European Space Agency, Noordwijk, Netherlands

*Corresponding Author: zeno.pavanello@unipd.it

Abstract

The potentialities of In-Orbit Servicing (IOS) to extend the operational life of satellites and the need to implement Active Debris Removal (ADR) to effectively tackle the space debris problem are well known among the space community. Research on technical solutions to enable this class of missions is thriving, also pushed by the development of new generation sensors and control systems. Among private companies, space agencies and universities, the European Space Agency (ESA) has been developing technologies in this field for decades. Several solutions have been proposed over the years to safely capture orbital objects, the majority relying on robotic systems. A promising option is the employment of an autonomous spacecraft (chaser) equipped with a highly dexterous robotic arm able to perform the berthing with a resident space object. This operation poses complex technical challenges both during the approach phase and after contact. In this respect, the design of an effective, reliable, and robust Guidance, Navigation and Control (GNC) system, for which several algorithmic architectures and hardware configurations are possible, plays a key role to ensure safe mission execution.

This work presents the outcomes of a research activity performed by a consortium of universities under contract with ESA with the goal to develop the navigation and control subsystems of a GNC system for controlling a chaser equipped with a redundant manipulator. Both the final approach until capture and the target stabilization phase after capture are considered in the study. The proposed solution aims at the implementation of a combined control strategy. Robust control methods are adopted to design control laws for the uncertain, nonlinear dynamics of the chaser and of the complete chaser–target stack after capture. Visual–based solutions, i.e., relying on active/passive electro–optical sensors, are selected for relative navigation. A complete sensor suite for relative and absolute navigation is part of the GNC system, including transducers for robot joint measurements. To properly validate the proposed solutions, a complete numerical simulator has been developed. This software tool allows to thoroughly assess the system performance, accounting for all the relevant external disturbances and error sources. A realistic synthetic image generator is also used for relative navigation performance assessment. This paper presents the design solutions and the results of preliminary numerical testing, considering three mission scenarios to prove the flexibility of the solution and its applicability to a wide range of operational cases.

Keywords: Close Proximity Operations, Space manipulator combined control, Relative navigation algorithm, GNC.

Acronyms

ADR Active Debris Removal.

C/E Chaser to End Effector.

CMG Control Moment Gyro.

CPO Close Proximity Operation.

CW Clohessy-Wiltshire.

DoF Degrees of Freedom.

ECI Earth Centered Inertial.

EE End Effector.

EGM2008 Earth Gravity Model 2008.

EKF Extended Kalman Filter.

EO Electro-Optical.

ESA European Space Agency.

ExGIT Extended Generalized Inertia Tensor.

FES Functional Engineering Simulator.

G/E Grasping Point to End Effector.

GEO Geostationary Earth Orbit.

GNC Guidance Navigation and Control.

GNSS Global Navigation Satellite System.

IGRF-13 International Geomagnetic Reference Field.

IMU Inertial Measurement Unit.

IOS In-Orbit Servicing.

LAR Launch Adapter Ring.
LED Light Emitting Diodes.
LEO Low Earth Orbit.
LFT Linear Fractional Transformation.
LIDAR Laser Detection and Ranging.
MED Momentum Exchange Device.
MEKF Multiplicative Extended Kalman Filter.
MoI Moment of Inertia.
NASA National Aeronautic and Space Administration.
PANGU Asteroid Natural Scene Generation Utility.
PnP Perspective-n-Point.
PoI Product of Inertia.
PWPFM Pulse Width Pulse Frequency Modulator.
RMS Root Mean Square.
T/C Target to Chaser.
TOF Time Of Flight.

1. Introduction

In the past decade, the interest of the space community towards new key technologies capable of solving problems like space debris or spacecraft failures has constantly grown. In this frame, new Close Proximity Operations (CPO) mission concepts such as In-Orbit Servicing (IOS) [1] and Active Debris Removal (ADR) [2] have been investigated. IOS missions aim to perform space operations such as up-close inspection, refuelling, repairing and upgrading with the goal of prolonging the operative life of another resident space object. As a consequence, IOS missions can be seen as a possibility for the satellite owners and operators to increase the return of investment by extending the life of the existing space assets, but could also represent a solution in addressing the space debris problem. In the past years, a number of missions have been studied [3]–[5], some even including tethered systems [6], [7] and some have recently flown¹ or are close to be launched² to prove IOS enabling technologies. Regarding the space debris problem, ADR missions offer a possibility to hold back the Kessler syndrome while also freeing usable orbital spots. The execution of both IOS and ADR missions requires an accurate and robust performance of the system. In particular, the main technical challenges of these missions are related to the design of the Guidance, Navigation and Control (GNC) system. If a space manipulator is employed during the capture phase, the GNC aspects become even more crucial, given the physical interaction between the robotic arm and the satellite itself.

In this framework, ESA has signed a contract with a consortium of three Italian universities to carry out a study on enabling technologies for the capture of a resident space object using a robotic arm. Specifically, the

team is composed by the University of Padua, the University of Naples “Federico II” and the Polytechnic of Milan. The goal of this study is double. On the one hand, it aims at developing innovative algorithms for (i) combined control of a chaser equipped with a highly dexterous robotic arm, and (ii) target-chaser relative navigation exploiting active or passive Electro-Optical (EO) sensors. On the other hand, a complete simulation environment used to support the development and testing of the mentioned technologies is under development. This simulation tool is called Functional Engineering Simulator (FES). The FES will feature a reusable modular structure making it a valuable design tool for GNC related technologies in the framework of orbital proximity operations, even beyond the specific applications developed in this study [8].

2. Problem definition

An IOS/ADR mission typically involves a chaser spacecraft, equipped with a set of actuators and sensors, which needs to approach and perform operations on a target spacecraft. These missions usually consist of seven phases: (i) Orbit transfer and phasing, (ii) Far-Mid range rendezvous, (iii) inspection, (iv) close range rendezvous, (v) reach and capture, (vi) target stabilization, (vii) servicing/deorbiting.

The focus of this study is on the fifth and sixth phases: reach and capture and target stabilisation. In the former the GNC system guides the chaser through a rendezvous manoeuvre up to a very short distance from the target, while the robotic arm reaches and grasps the target on the selected capture point. In the latter the chaser consolidates the stack and performs a stabilisation manoeuvre to achieve the damping of the residual angular rates. In both phases, the design of the navigation and control subsystems is strongly affected by the degree of cooperation and collaboration of target. The definitions of the cooperativeness and collaboration of the target are reported in Table 1.

According to these definitions, three representative IOS and ADR scenarios have been defined focusing on the challenges posed by the lack of cooperativeness and collaboration for space robotics operations. The three default scenarios under study are reported in Table 2. To have a reference scenario for one of the most common IOS operations, Scenario 1 includes a Nadir Pointing GEO satellite that mounts easily detectable fiducial markers. Finally, Scenario 3 exemplifies the most challenging situations in terms of GNC design, being representative of an ADR mission tailored to the largest debris in orbit, ENVISAT. The infamous dismissed spacecraft has been selected due to the large number of available studies that were carried out in the past, which will be used as a benchmark for comparison. It does not present any fiducial marker which can aid in the navigation process and it is uncontrollably spinning with an absolute residual velocity of 5 deg/s.

¹<https://news.northropgrumman.com/news/releases/northrop-grumman-successfully-completes-historic-first-docking-of-mission-extension-vehicle-with-intelsat-901-satellite>

²<https://clearspace.today/>

Table 1. Definition of *collaborativeness* and *cooperativeness* for close-proximity operations.

Target Type	Description
Cooperative	The target can provide direct information about its relative states in real-time on-board to the servicer to aid the relative navigation task.
Semi-cooperative	The target can provide indirect information about its relative states to the servicer through exploitation of active/passive markers.
Non-cooperative	The target does not offer any support for the relative navigation.
Collaborative	The target can actively and accurately maintain an attitude profile that can aid the approach and docking/capture process.
Semi-collaborative	The target can actively keep an attitude profile to aid the approach but not accurately enough to aid the docking/capture process, i.e., only coarse attitude control is operative.
Non-collaborative	The target attitude is uncontrolled and it cannot aid the capture operation in any way.

Like in the first scenario a dedicated grasping point is not mounted on the spacecraft, leaving the LAR as the only reasonable choice to be considered for the capture.

The chaser architecture is similar throughout the three scenarios. The spacecraft mass is proportional to the mass of the target; in Scenario 1 it also comprises two large solar arrays, while in Scenario 2 and 3 the solar panels are body mounted, to favour the agility to reach the required angular rates. For the attitude control, a set of Momentum Exchange Devices (MEDs) is mounted on the spacecraft: specifically a pyramid of four high torque Control Moment Gyros (CMGs) in Scenario 3 and four Reaction Wheels mounted in the NASA standard configuration in Scenarios 1 and 2. PWPFM thrusters are used to execute orbital manoeuvres and to desaturate the MEDs when necessary. The chaser absolute state estimation is guaranteed throughout the scenarios by means of an IMU, a star tracker and a GNSS receiver, the measures of which are filtered using standard techniques like EKF filtering, while the relative navigation function is entrusted to electro-optical sensors. The robotic arm is mounted on one side of the spacecraft and it is composed of 7 revolute joints, thus having 7 Degrees of Freedom (DoF). The length of the links varies according to the scenario.

An important aspect of the problem and one of the reasons that make this kind of study of particular interest is the large variety of situations and targets that can be involved in ADR operations. Dismissed orbiting spacecraft are very diverse in terms of orbit, size, shape and dynamic properties, thus a proper tool to study these types of missions should be expected to be flexible and adaptable to a variety of different scenarios. Starting from the three that were presented in this section, the outcome of the project is intended to be a tool which includes flexible GNC modes, namely the FES, that can be applied to any custom scenario, in order for the users to be able to study at a preliminary level the ADR mission involving any de-

sired target and using the preferred chaser architecture.

3. GNC system design and validation

The proposed combined control and relative navigation architectures for the three scenarios are illustrated in this section.

3.1 Combined control approach

As a preliminary step to the design of the controller, a rigid multibody model of the system has been developed. Such model includes the chaser platform and a 7 DoF redundant manipulator mounted on the spacecraft base. The equations of motion of the system have been obtained using standard methodologies applied in robotics. In the case under study, the floating version of the well-known recursive Newton-Euler algorithm for systems of rigid bodies [9] has been used as it ensures computational efficiency and it allows considering arbitrarily complex configurations. The spatial vector notation [10] has been adopted to naturally account for the coupling between translational and rotational dynamics. Unlike most of the previous studies in the space robotics field, an orbital disturbance term has been considered in order to evaluate possible undesired effects due to the coupling between multibody and orbital dynamics; this disturbance can be straightforwardly added in the model thanks to the recursive approach. This stated, the nonlinear equations of motion of the system can be cast in the following form

$$H(\mathbf{q}) \begin{bmatrix} \dot{\boldsymbol{\omega}}_b \\ \dot{\mathbf{v}}_b \\ \ddot{\mathbf{q}} \end{bmatrix} + \mathbf{C}(\boldsymbol{\omega}_b, \mathbf{v}_b, \dot{\mathbf{q}}, \boldsymbol{\eta}_b, \mathbf{r}_{b/t}, \mathbf{q}, t) = \begin{bmatrix} \mathbf{M}_b \\ \mathbf{F}_b \\ \boldsymbol{\tau} \end{bmatrix} \quad (1)$$

where $\boldsymbol{\omega}_b, \mathbf{v}_b \in \mathbb{R}^3$ are base angular and linear velocity, respectively, $\mathbf{q} \in \mathbb{R}^7$ is the vector of joint angles, $\boldsymbol{\eta}_b \in \mathbb{S}^3$ is the unit quaternion describing the base attitude with $\mathbb{S}^n = \{\mathbf{v} \in \mathbb{R}^{n+1} : \|\mathbf{v}\| = 1\}$, $\mathbf{r}_{b/t} \in \mathbb{R}^3$ is

Table 2. Scenarios definition.

Scenario	Mission Type	Cooperativeness	Collaborativeness	Target	Orbit
SC 1	IOS	Semi-cooperative	Semi-collaborative	SSL-1300 GEO platform	GEO
SC 2	ADR	Semi-cooperative	Non-collaborative	Arrow platform (OneWeb)	LEO
SC 3	ADR	Non-cooperative	Non-collaborative	ENVISAT	LEO

the position of the base with respect to the target, while $\mathbf{M}_b, \mathbf{F}_b \in \mathbb{R}^3$ and $\boldsymbol{\tau} \in \mathbb{R}^7$ are base torque, force and joint motor torque, respectively. $H \in \mathbb{R}^{13 \times 13}$ is the joint space inertia matrix, while $\mathbf{C} \in \mathbb{R}^{13}$ is the Coriolis/centrifugal term; it is worth noting that, because of the relative orbital dynamics, the latter depends on the chaser base position and attitude and it may also depend on time in the case of elliptical orbits. Concerning the post-capture phase, the target is rigidly attached to the EE. In this case, the stacked configuration (chaser + manipulator + target) can be thought of as a unique multibody system where the last link inherits the inertial parameters of the target. Since in the post-capture phase the position of the base of the stack is not controlled and base body forces are not generated, the system conserves the linear momentum and equation Eq. (1) is modified to include the conservation of linear momentum [11].

As for control design, a combined approach is proposed wherein base and manipulator states are controlled together, following ideas recently proposed in the literature. The combined architecture has several advantages over decoupled control strategies, from fuel efficiency to performance improvement. Both linear and nonlinear design methods have been considered [12]–[17]. Generally speaking, linear design methods provide tools for the systematic robust tuning of controllers. On the other hand, nonlinear control design methods provide stability guarantees in a larger domain, but it is often quite difficult to systematically tune the controller to satisfy performance and robustness requirements. The proposed control approach consists in using nonlinear controllers whose free parameters (e.g., the PD gains of the feedback part) are tuned by first linearizing the plant and the control law and then by leveraging the structured H_∞ framework [18]. In this manner, it is possible to ensure stability for the nonlinear system while imposing local performance requirements on the resulting closed-loop about the desired configurations at design time. In addition, it is also possible to make assessments on robustness exploiting the structured singular value framework.

Concerning the control architecture, both joint space and task space controllers have been investigated [17]. The former aims at controlling the joint angles of the manipulator, which are appropriately commanded via the inverse kinematics to track a desired EE pose; the latter

directly controls the EE pose. Manipulator redundancy is tackled in both architectures by leveraging the existing approaches from the literature [19]–[23]. The joint space control law is given by

$$\begin{bmatrix} \mathbf{M}_b \\ \mathbf{F}_b \\ \boldsymbol{\tau} \end{bmatrix} = \tilde{\mathbf{C}}(\boldsymbol{\omega}_b, \mathbf{v}_b, \dot{\mathbf{q}}, \mathbf{q}) + \tilde{H}(\mathbf{q}) \begin{bmatrix} \mathbf{a}_\eta \\ \mathbf{a}_r \\ \mathbf{a}_q \end{bmatrix}, \quad (2)$$

where $\tilde{\mathbf{C}}, \tilde{H}$ are the estimates of Coriolis/centrifugal term and mass matrix, respectively and $\mathbf{a}_\eta, \mathbf{a}_r \in \mathbb{R}^3, \mathbf{a}_q \in \mathbb{R}^7$ are the virtual control inputs based on PD laws [17]. Similarly to [15], the task space control law is defined as

$$\begin{bmatrix} \mathbf{M}_b \\ \mathbf{F}_b \\ \boldsymbol{\tau} \end{bmatrix} = \begin{bmatrix} I_6 & A_{eb}^T(\mathbf{q}) & J_{nb}^T(\mathbf{q}) \\ 0_{7,6} & J_e^T(\mathbf{q}) & J_{nm}^T(\mathbf{q}) \end{bmatrix} \begin{bmatrix} \mathcal{F}_b \\ \mathcal{F}_e \\ \xi_n \end{bmatrix}, \quad (3)$$

where $A_{eb} \in \mathbb{R}^{6 \times 6}$ is the adjoint operator from end-effector frame to chaser base frame, $J_e(\mathbf{q}) \in \mathbb{R}^{6 \times 7}$ is the end-effector Jacobian, $J_n(\mathbf{q}) = \begin{bmatrix} J_{nb} & J_{nm} \end{bmatrix} \in \mathbb{R}^{1 \times 13}$ is a map relating the robot velocities to the null space velocity and $\mathcal{F}_b, \mathcal{F}_e \in \mathbb{R}^6, \xi_n \in \mathbb{R}$ are virtual control inputs based on PD laws for base pose, end-effector pose and null-space motion, respectively.

In both architectures, base pose and generalized velocity feedback are necessary to coordinate base and manipulator control tasks. The controller outputs are the control wrench of the base and the joint torques of the robotic arm.

As mentioned above, the control problem is formulated using the structured H_∞ approach. Simplified performance specifications and control moderation requirements are imposed by augmenting the plant using frequency weights for the sensitivity and control sensitivity functions as shown in Fig. 1. In this figure, the block G' denotes the plant, while K' is the controller. The signal w denotes the setpoint (*i.e.*, desired base pose and joint angles), y is the corresponding control error, u is the control input and W_S, W_u are the sensitivity functions weighting control error and control input, respectively. The linearized system is modelled in Linear Fractional Transformation (LFT) form to account for uncertainties on mass

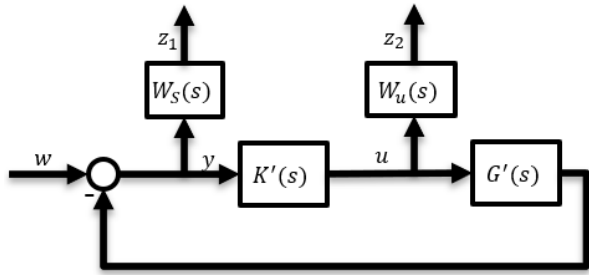


Fig. 1. Controller synthesis formulation.

and inertia parameters of chaser and target. In this setting, the controller can be robustly tuned in MATLAB using the advanced methodologies implemented in the systune routine [24]. The effects of unmodelled phenomena like sloshing and flexible appendages are analysed only after control design using μ -analysis [12]. Indeed, the linear control model must be modified by adding these additional effects and the corresponding uncertainties using the approach provided in [25]. A complete verification of the GNC considering various nonlinearities will be performed using the FES after controller design.

3.2 Relative navigation system

An optical-based relative navigation solution, i.e., relying on active and passive Electro-Optical (EO) sensors, has been selected to provide estimates of the relative rotational and translational state of the multibody system composed by the chaser and the robotic arm with respect to the target. This choice is motivated by the fact that the target is non-cooperative in all the scenarios under study, thus not allowing the use of differential Global Navigation Satellite Systems (GNSS)-based techniques, which would in any case be hindered by occlusion and multi-path phenomena when the vehicles orbit in close proximity to each other, e.g., during the reach and capture phase [26].

One critical design constraint for such operations is that the relative navigation function must be able to estimate the relative state of the chaser with respect to the target (T/C), as well as the relative state of the robotic arm EE with respect to the selected grasping point on the target surface (G/E). In this respect, several architectural options have been investigated in the literature, mainly differing in terms of the role played by sensors potentially installed on the robotic arm to support the grasping operations [27]–[29]. In this work, also following the results of the COMRADE project [29], the relative navigation function is entrusted to two EO sensors rigidly attached to the chaser main body and to the EE to carry out T/C and G/E relative state estimation, respectively. The idea to use the sensor attached to the robotic arm, not only for monitoring purposes but also to produce direct G/E pose estimates, is

critical to reduce the robotic arm ego motion uncertainty in the G/E relative state estimation process. This aspect is particularly important when dealing with tumbling targets.

A high-level block diagram of the proposed architecture is provided in Fig. 2. The configuration is loosely coupled meaning that the raw data produced by the EO sensors are processed within a separate block (i.e., outside of the filter) to get relative position and attitude measurements to be used in the correction step of the filtering schemes [30], [31]. Since the target is a known object, the inputs required by the main processing functions (red blocks) include target, chaser and robotic arm GEOMETRIC information (orange blocks), as well as the chaser absolute state estimates and the robotic arm’s joint sensors measurements (blue blocks). It is worth highlighting that the sensor attached to the robotic arm might not be correctly pointed toward the target during the entire reach and capture manoeuvre (especially while the arm is not fully deployed starting from its stowed configuration). So, to allow the G/E relative state estimation filter to be operational even in absence of direct G/E pose estimates, the latter is designed to also receive in input (i) the pose of the EE with respect to the base of the robotic arm (C/E) obtained by applying its forward kinematics model, (ii) the output of the T/C relative state estimation filter.

The T/C and G/E relative state estimates are used to feed the combined control function which provides in feedback chaser commands (e.g., thrusts) that can be used by the T/C relative navigation filter to compute the resulting accelerations acting on the chaser.

To carry out the selection of the body-mounted and robotic arm EO sensors, different options (namely monocular cameras, stereo cameras, and active LIDARs) have been investigated considering both technological and algorithmic aspects. On the one hand, passive systems have lower size and weight, and require less power supply than LIDARs, thus ensuring lower complexity to the relative navigation subsystem design. Also, they are typically characterized by a better angular resolution. On the other hand, LIDARs can provide direct target distance measurements without requiring the full pose estimation process to be completed (as in the case of monocular sensors), or complex and computationally expensive disparity map calculation (as in the case of stereo cameras). In addition, LIDAR-based systems have advantages in terms of illumination invariance. Based on this trade-off analysis and considering the availability of fiducial markers on the target surface in Scenarios 1 and 2, the result of the selection process is summarized in Table 3.

Monocular cameras represent a convenient solution for the semi-cooperative scenarios since they can robustly extract (detection) and recognize (identification) the fiducial markers installed on the target surface, while posing

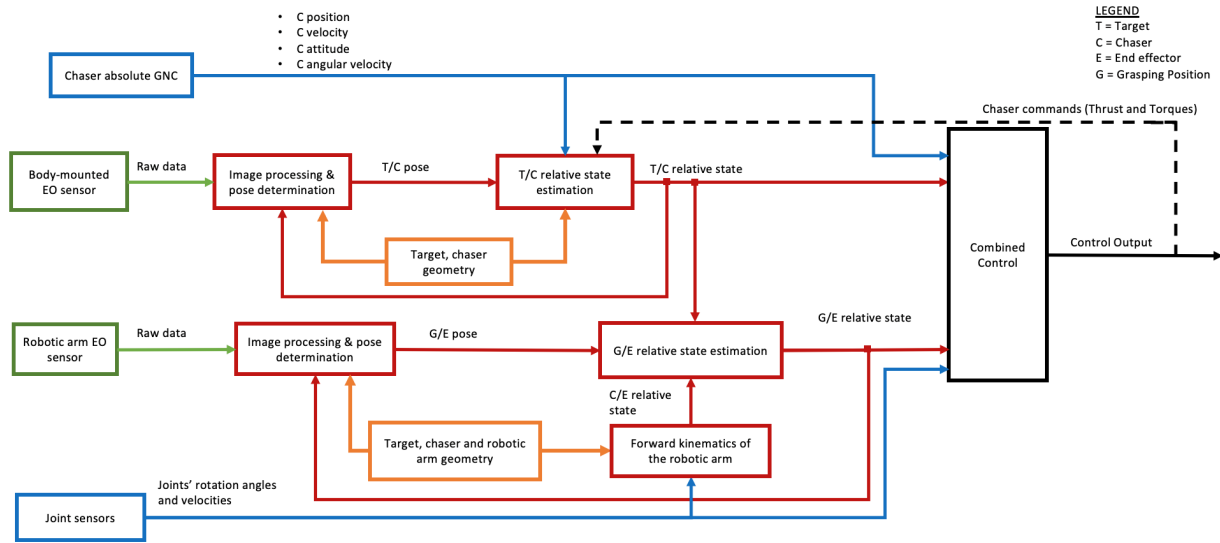


Fig. 2. High-level block diagram of the loosely coupled relative navigation architecture proposed in this study.

Table 3. Sensor selection for the scenarios under study.

Scenario	Chaser body	Robotic arm
SC 1	Monocular camera	Monocular camera
SC 2	Monocular camera	Monocular camera
SC 3	Flash LIDAR	TOF camera

limited design constraints. The resulting set of 2D-to-3D correspondences can then be used to get accurate pose estimates by solving the Perspective-n-Point (PnP) problem [32]. With regards to the detection step, the image processing approach is strongly dependent on the type of the marker, as a large variety of different solutions can be employed, including

- passive visual markers (obtained by covering the target surface with paintings or coatings with *ad-hoc* reflectivity);
- semi-passive retroreflectors (despite not requiring a dedicated power supply on the target, such scenario must foresee an active illumination source on the chaser);
- Active Light Emitting Diodes (LEDs).

Retroreflectors and LEDs can be separated from the background by searching for very bright objects in the scene. Instead, the detection of visual markers must rely on more complex image processing techniques taking advantage of their specific shape rather than only relying on their brightness.

In the first scenario, a set of ten retroreflectors (nine coplanar and one mounted with an offset in the surface

outer normal direction), illuminated by an infrared laser source on the chaser, is selected as target for the body mounted camera. Indeed, this is a robust and safe solution for the servicing of a high-value GEO asset. The number of retroreflectors ensures an adequate redundancy (in case the target is not approached with nominal attitude) and avoids sudden performance degradation when single retroreflectors fall outside of the FOV. Instead, the robotic arm camera is designed to detect a set of three white circular markers on a black background (similarly to the concept of concentric contrasting circles [33]). In this case, the possibility to minimize the number of correspondences is motivated by the fact that an accurate initial guess of the G/E pose is provided to the PnP solver by combining the T/C and C/E relative state estimates in the prediction step of the G/E filter.

In the second scenario, code-based visual markers are selected since they represent a promising solution for standard-designed targets like the elements of a large LEO constellation. Specifically, one $20 \times 20 \text{ cm}^2$ Aruco marker [34] is placed at the centre of each target face (excluding those hosting the solar panels along which the approach is not feasible), while one $5 \times 5 \text{ cm}^2$ Aruco marker is placed close to the grapping interface.

After detection, the markers must be recognized, i.e., their pixel coordinates must be matched with available information on the target Geometry (e.g., their 3D position vector in target-fixed coordinates). Considering that an *a-priori* knowledge of the relative state parameters is available both at the start of the reach and capture phase (in the acquisition mode) and at any sub-subsequent time frame (i.e., as the output of the prediction step of the filters), the identification can be done by reprojecting the markers

on the image plane and exploiting the Nearest Neighbour approach. Finally, a non-linear least square PnP solver, based on the Levenberg-Marquardt algorithm [35], is implemented for pose estimation.

With regards to the third scenario, the need to have direct distance estimates is considered a critical constraint when dealing with non-cooperative and tumbling targets. Hence, relative navigation is entrusted to active systems able to produce 3D point clouds from the imaged scene. Specifically, a high-performance Flash LIDAR is selected as body-mounted sensor, because it suffers from motion blur phenomena arising from quick relative dynamics less than scanning systems, while the use of a TOF camera is considered more compatible with the installation constraints on the robotic arm [36]. For both these sensors, a customized implementation of the Iterative Closest Point algorithm [37] is selected to provide accurate T/C and G/E pose estimates by registering the measured point cloud to the one obtained by discretizing a CAD model of the target Geometry.

Concerning the filtering scheme, a Multiplicative Extended Kalman Filter (MEKF) is selected for both the T/C and G/E relative state estimation tasks in all the scenarios under study. Indeed, this type of filter allows dealing with non-linear systems dynamics, and it is easily implementable. Also, the multiplicative formulation allows avoiding singularities in the covariance matrix due to the unit-norm constraint characterizing quaternion which are used for relative attitude parametrization. As a final remark, it is worth highlighting that the T/C filtering scheme is designed to output the absolute angular velocity of the target rather than the T/C relative angular velocity.

3.3 Functional Engineering Simulator

The simulation support for the testing and validation of the Guidance and Navigation technologies is mainly developed in the MATLAB/Simulink environment producing as an output a highly modular and flexible tool, namely the Functional Engineering Simulator (FES).

In the Simulink model, the dynamics of the chaser, target and robotic arm are represented using the Simscape Multibody package [38], which is also coupled with a useful mechanical visualizer as shown in Fig. 3. This allows the developer to focus on the modeling of the physical phenomena *per se*, without having to worry about the correct formulation of the complex differential equations which govern the kinematics and the dynamics of the single bodies. Moreover, using Simscape Multibody a large number of rigid bodies can be modularly defined and connected using a variety of different joints. Hence, the target spacecraft is composed of a central prismatic bus which is welded in series to one or more bodies representing the solar panels, while the chaser spacecraft is connected in addition to the robotic manipulator. This last component

is made of 7 cylindrical links, connected to each other by revolute joints, which only allow a 1 DoF rotation.

Simscape Multibody was also found to be suitable to simulate the orbital dynamics of the spacecraft. By means of a fictitious 6 DoF joint, the two spacecraft can be separately connected to the ECI frame (centered in the center of the Earth). By applying the correct gravitational attraction, the two bodies gravitate according the real orbital parameters and the relative motions between the two satellites is automatically reproduced with an acceptable degree of error without the need of using the CW equations of motion.

Regarding the rest of the environmental aspects, a full model has been implemented in the FES for each of the relevant phenomena. The user is given the option to activate or deactivate the contributions reported in Table 4, with the exception of the first harmonic of the gravity field. To comply with the multibody approach, external perturbations are applied to every component of the system as external forces and torques; hence, if a satellite equipped with deployed solar panels is considered, the perturbations act not only at the center of mass of the satellite, but also at the center of mass of the appendages. In addition, non-linear models are considered in the simulation such as flexibility of structure and sloshing, which can also be enabled/disabled, depending on the specific needs of the user.

In particular, the flexible structures, such as the solar panels and the manipulator links, are modelled by means of a set of Simscape Multibody blocks. A slightly more complex modeling effort has been carried on to simulate the sloshing phenomenon affecting the spacecraft tanks: the parameters of an equivalent mechanical model comprising a 3 DoF pendulum are programmatically computed, given the input by the user on tank size, fill ratio and liquid physical characteristics [39].

In the FES, Guidance and Navigation operations are simulated by implementing the control techniques de-

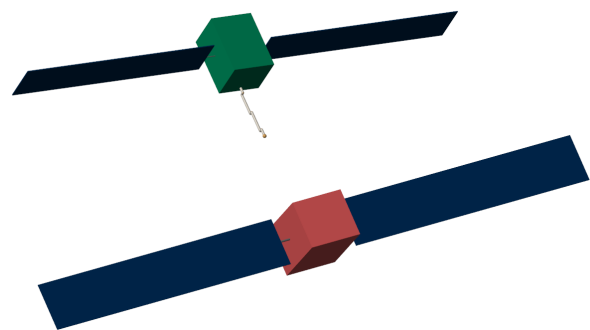


Fig. 3. Mechanics Explorer representation of the chaser satellite approaching the target.

Table 4. Environment models

Phenomenon	Model
Gravity Field	EGM2008 [40]
Geomagnetic Field	IGRF-13 [41]
Gravity Gradient	1 st order approximation [42]
Third body attraction	Astronomical Almanac [43]
Atmospheric Drag	NRLMSISE-00 [44]
Solar Pressure	Newtonian specular and diffusive model [45]

scribed in Section 3.1, the Relative Navigation Filter described in Section 3.2, and several sensors and actuators reproducing the real hardware behaviour. A set of non-linear actuators and sensors models has been developed. In particular, the actuators include Momentum Exchange Devices, i.e., reaction wheels and Control Moment Gyros CMGs, thrusters and DC motors for the arm links. The sensors include GNSS receivers, Star Trackers, Inertial Measurement Units (IMU) and optical encoders for the arm links. Data from monocular cameras and LIDAR are realistically reproduced using the ESA Planet and Asteroid Natural Scene Generation Utility (PANGU) Tool.

The FES is able to simulate the capture phase of different targets in different scenarios and the dynamics of the stack after the capture. The transition between the two phases is achieved via an analytical formulation, to ensure consistency of the invariant quantities when switching from two independent orbital assets to the stack (unique) configuration. Following the work of Yoshida and Umetani [46], [47] and considering that the complex simulation of the contact dynamics is of no interest, the Extended Generalized Inertia Tensor (ExGIT) method is used to compute the state (position and velocity) of the complete stack and of the manipulator joints, given the state of the two spacecraft and of the manipulator right before capture.

4. Numerical results

In the present section the preliminary results of the open loop simulations of the combined control and relative navigation algorithms are presented.

4.1 Control system performance

In this section, the results of the control design of Scenario 2 are illustrated. As described in Section 3.1, two control architectures were originally considered. As satisfactory results have not been achieved when performing the synthesis of task space controllers in the presence of measurement delays, it has been decided to focus only on the joint space controller architecture. The main reason

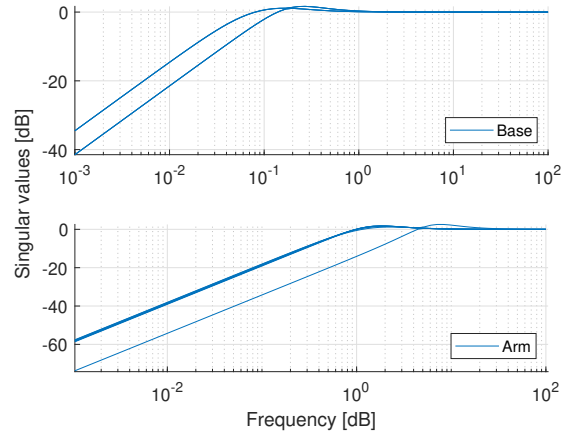


Fig. 4. Closed-loop sensitivity functions, pre-capture. From base desired pose to base pose (Top). From desired joint angles to joint angles (bottom).

Table 5. Chaser and target uncertainties.

Parameter	Nominal	Variability
Ch. Mass [kg]	372	±5%
Ch. MoI [kg m ²] (x,y,z)	200, 200, 140	±10%
Ch. PoI [kg m ²]	0	±1
Ch. CoM [m] (x,y,z)	0	±0.05
Ch. Slosh. freq. [rad/s]	0.0063	±20%
Ch. Slosh. damp.	0.001	±40%
Tg. Mass [kg]	150	±10%
Tg. MoI [kg m ²] (x,y,z)	45, 20, 50	±20%
Tg. PoI [kg m ²]	0	±1
Tg. CoM [m] (x,y,z)	0	±0.05

for this difference in performance is due to the different structure of the controllers and to the different delays affecting the estimates used by the feedback. The bandwidth of the linearized control system is imposed considering requirements of similar missions in the literature [4]. The achieved sensitivity functions for base pose and arm joint tracking are shown in Fig. 4.

After synthesis, robustness with respect to rigid-body uncertainties such as mass, moments of inertia (MoI), products of inertia (PoI) and centre of mass (CoM) position and sloshing listed in Table 5 is assessed using μ -analysis.

In the presence of sloshing, the LFT is too complex to achieve reliable robust stability results. To overcome this problem, the following approach has been used: sloshing uncertain parameters (i.e., sloshing frequency ω_n and damping ζ_s) are gridded within the uncertain set and for

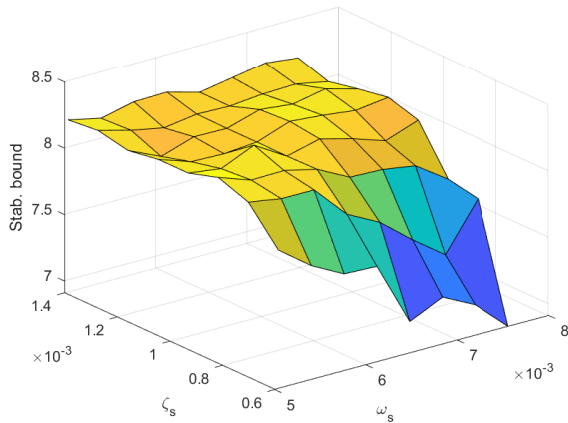


Fig. 5. Gridding approach results: lower bound of the stability margin.

any point on the grid robust analysis is performed considering all the other parameters as uncertain. A grid of 8×8 equally spaced points is selected. In this case, the robust analysis problem translates into computing 64 stability margins (i.e., 64 computations of the bounds of the structured singular value). The results of the analysis are shown in Fig. 5, in which the stability margin³ of any point of the grid is reported: the robust stability for any evaluation is confirmed.

The designed joint space control solution has been assessed via nonlinear simulations in Simulink considering the nonlinear rigid body dynamics, actuators saturation and thrusters discretization. For these tests, a preliminary solution of the guidance has been used to generate the reference signals to track: the base performs station-keeping w.r.t. the target, while the EE moves to grasp the grapple fixture as shown in Fig. 6, in which the error between the EE gripper and target grasping point is reported. Figure 7 shows the time history of the control inputs: it can be seen that in order to guarantee end-effector tracking and base station-keeping, all the actuators must be used. The sudden variation of the control inputs at 25 s is due to the guidance algorithm which changes its logic when the end-effector has been aligned with the target. These results show that the controller is capable of tracking representative guidance references while keeping the control errors small.

Concerning post-capture control, the controller is designed to track a desired base angular rate and joint angles profile (to ensure a successful rigidisation of the stack) and the obtained sensitivity functions are shown in Fig. 8. The control bandwidth is selected to ensure appropriate detumbling times as imposed by mission constraints.

³The stability margin is the inverse of the structured singular value μ . Robust stability is ensured if its lower bound is greater than 1.

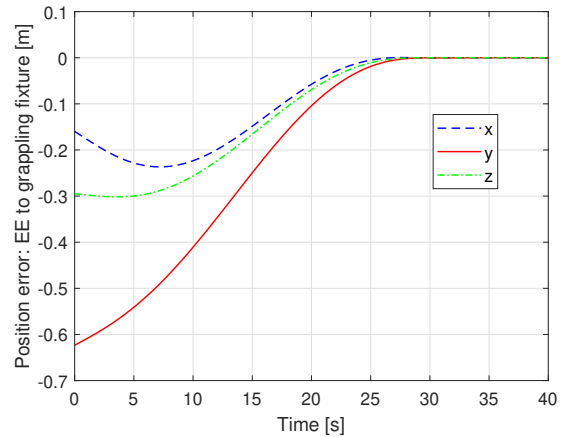


Fig. 6. EE to grasping point position error.

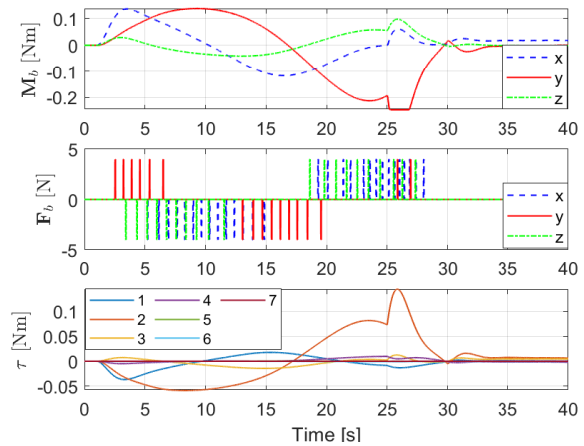


Fig. 7. Control inputs in the reach and capture phase.

Concerning robustness analysis, the lower and upper bounds of the stability margin for the complete LFT are 1.01 and 1.7, respectively. In this case, robust stability can be assessed without using the sub-optimal gridding analysis as the lower bound is greater than 1.

4.2 Relative navigation performance

While an intense campaign of numerical simulations is currently ongoing to thoroughly assess at unit level the performance of the architecture described in Section 3.2 for all the scenarios under study, preliminary results are reported in this section for Scenario 1. To this aim, an R-bar final approach trajectory of the chaser toward the target has been defined, during which the distance between the body-mounted camera and the target face hosting the LAR varies from 6.8 m to 1.9 m. The chaser attitude is assumed to be controlled so that the target (and the fiducial markers on its surface) is safely kept in the sensor FOV. This assumption is reasonable considering

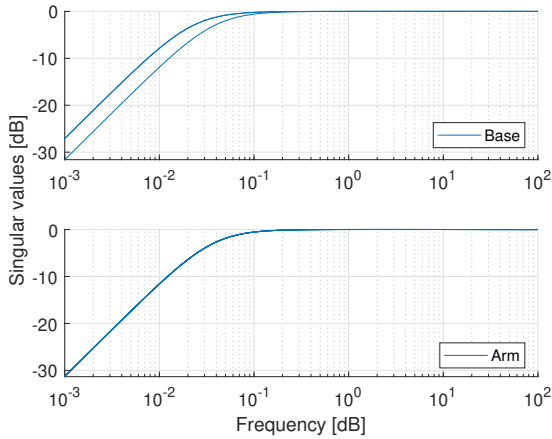


Fig. 8. Closed-loop sensitivity functions, post-capture. From desired angular rate to angular rate (top). From desired joint angles to joint angles (bottom).

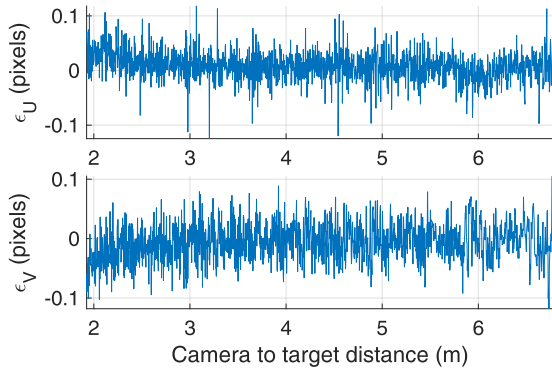


Fig. 9. Time variation of the centroiding error averaged over all the detected retroreflectors. Scenario 1. Body mounted camera.

the semi-collaborative nature of the target. Finally, the nominal motion of the robotic arm is obtained solving the inverse kinematics problem by setting constraints on the fiducial markers visibility and on the final position of the EE (which must coincide with the selected capture point). Performance assessment over such trajectory is carried out by running a set of 100 numerical simulations. For each run, the error in the knowledge of the initial relative state parameters and of the camera intrinsic calibration parameters is extracted from zero-mean Gaussian distributions with standard deviations reported in Table 6.

The output of the chaser absolute navigation filter is also simulated by adding a time correlated error to each component of the true state. This error is obtained by passing a zero-mean Gaussian noise through a discrete-time low-pass filter. The standard deviation of this noise

Table 6. Uncertainty level in the knowledge of the relative state at scenario start, and of the camera intrinsic calibration parameters.

Parameter	Uncertainty level (1σ)
Relative position	5 cm (along-boresight) 1.7 cm (cross-boresight)
Relative attitude	1 deg (each axis)
Relative velocity	3.3 mm/s (each axis)
Relative angular velocity	0.033 deg (each axis)
Focal length	1 pixel
Principal point	1 pixel

Table 7. Uncertainty level in the knowledge of the chaser absolute navigation state.

Parameter	Uncertainty level (1σ)
Position	30 m
Attitude	0.0017 deg (each axis)
Velocity	0.5 m/s (each axis)
Angular velocity	0.017 deg

is reported for each parameter in Table 7.

The image processing approaches designed for the body-mounted and robotic arm cameras have shown capability to detect both the retroreflectors and the visual markers with sub-pixel accuracy level over the entire trajectory. For instance, Fig. 9 shows the horizontal (ϵ_U) and vertical (ϵ_V) components of the centroiding error for the retroreflectors averaged over all the detections. Specifically, the instantaneous error value for each detection is computed as the difference between the detected image coordinates of the retroreflector and their reprojection based on the true pose parameters.

Such image processing performance allows obtaining sub-millimetre and cents of degree level accuracy in the relative position and attitude estimation, respectively. This is shown in Fig. 10 where ΔX , ΔY and ΔZ are the errors in estimation of the relative position vector components, while $\Delta\gamma$, $\Delta\beta$ and $\Delta\alpha$ are the errors characterizing the elements of a 321 sequence of Euler angles parametrizing the relative attitude.

Figure 10 also shows that (i) the relative position accuracy improves in all the components at shorter distance as a consequence of the better spatial resolution; (ii) the estimate of the along-boresight component is slightly less accurate than the cross boresight one, which is to be expected considering that depth is not a direct observable of a monocular camera system; (iii) the relative attitude ac-

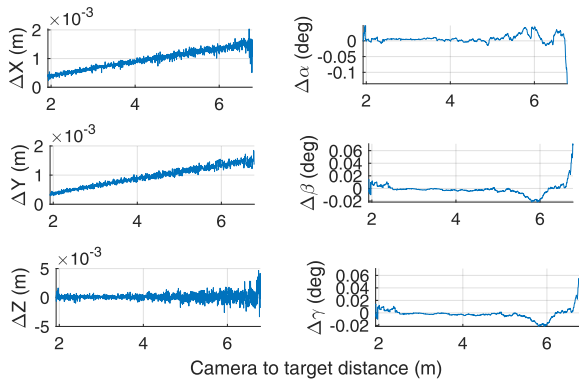


Fig. 10. Time variation of the pose estimation error. Scenario 1. Body mounted camera.

curacy remains constant along the approaching trajectory after convergence.

Finally, the results obtained by the proposed architecture in terms of T/C and G/E relative state estimation are statistically summarized in Table 8.

Table 8. Root Mean Square (RMS) of the error in the T/C and G/E relative state estimates evaluated over the entire approaching trajectory. Results are averaged over 100 simulations.

Relative navigation output	RMS
T/C relative position	0.05 cm
T/C relative attitude	0.08 deg
T/C relative velocity	0.46 mm/s (each axis)
T angular velocity	2.01×10^{-5} deg/s
G/E relative position	0.09 cm
G/E relative attitude	0.02 deg
G/E relative velocity	0.22 mm/s
G/E relative angular velocity	2.01×10^{-4} deg/s

5. Conclusions

This paper presented preliminary design activities concerning the development of innovative relative navigation and combined control approaches to support the capture and the stabilization of space targets using a chaser equipped with a robotic arm in the frame of Close Proximity Operation scenarios. The combined control approach is based on a non-linear controller the free parameters of which are tuned by linearizing the plant and the control law. The joint-space controller approach has been preferred to the task-space one because it performs better in the presence of time delays. The relative navigation architecture relies on the presence of fiducial markers or recog-

nizable geometric properties on the target, which are detected by active and passive EO sensors mounted on both the chaser body and on the robotic arm EE. In order to cover the main challenges of CPOs, three scenarios have been defined which are representative of (i) an In-Orbit Servicing mission to a GEO communication satellite; (ii) a deorbiting mission of a large constellation LEO satellite; (iii) an Active Debris Removal mission targeted to ENVISAT. Open loop preliminary control and navigation results were presented regarding the first two scenarios. These results show capability to meet the specifications imposed by the requirements of the project.

A test plan is currently under development to assess the robustness of the developed solutions via the implementation of the developed GNC algorithms in a Functional Engineering Simulator via standard and Montecarlo analysis. The FES will be capable of representing the mission scenarios accounting for the multibody coupling phenomena and the environmental perturbations and including realistic models of sensors and actuators. The FES is currently being integrated with the overall GNC architecture in closed loop. Thanks to its modularity and its flexibility, it will serve as a key tool to support design of future missions involving close-proximity operations.

References

- [1] A. Flores-Abad, O. Ma, K. Pham, and S. Ulrich, "A review of space robotics technologies for on-orbit servicing," *Progress in Aerospace Sciences*, vol. 68, pp. 1–26, 2014.
- [2] C. Bonnal, J. M. Ruault, and M. C. Desjean, "Active debris removal: Recent progress and current trends," *Acta Astronautica*, vol. 85, pp. 51–60, 2013.
- [3] Rank P., Q. Mühlbauer, W. Naumann, and K. Landzettel, "The Deos Automation and Robotic Payload," in *Proceedings of the Symposium on Advanced Space Technologies in Robotics and Automation*, 2011.
- [4] S. Estable, C. Pruvost, *et al.*, "Capturing and de-orbiting Envisat with an Airbus Spacetug . Results from the ESA e.Deorbit consolidation phase study," *Journal of Space Safety Engineering*, vol. 7, pp. 52–66, 2020.
- [5] A. Caon, F. Feltrin, *et al.*, "Ground facility for validation of proximity operations: A hardware-in-the-loop experiment," Jul. 2020.
- [6] R. Mantellato, L. Olivieri, and E. C. Lorenzini, "Study of dynamical stability of tethered systems during space tug maneuvers," *Acta Astronautica*, vol. 138, pp. 559–569, 2017.

- [7] L. Olivieri, A. Valmorbidia, *et al.*, “Test of Tethered Deorbiting of Space Debris,” *Advances in Astronautics Science and Technology*, vol. 3, no. 2, pp. 115–124, 2020.
- [8] R. Opromolla, F. Branz, *et al.*, “Chaser-Robotic Arm Combined Control and Optical Relative Navigation for Space Target Capture,” in *XXVI International AIDAA Congress*, 2021, p. 11.
- [9] E. Stoneking, “Newton-Euler Dynamic Equations of Motion for a Multi-body Spacecraft,” in *Proceedings of the AIAA GNC Conference*, 2007.
- [10] R. Featherstone, *Rigid Body Dynamics Algorithms*. Springer-Link, London, 2008.
- [11] Y. Umetani and K. Yoshida, “Resolved motion rate control of space manipulators with generalized Jacobian matrix,” *IEEE Transactions on robotics and automation*, vol. 5, no. 3, pp. 303–314, 1989.
- [12] G. Dullerud and F. Paganini, *A Course in Robust Control Theory: A Convex Approach*. Springer, 2000.
- [13] F. Aghili, “Coordination Control of a Free-Flying Manipulator and Its Base Attitude to Capture and Detumble a Noncooperative Satellite,” in *Proceedings of the IEEE/RSJ International Conference on Intelligent Robots and Systems*, 2009.
- [14] A. M. Giordano, A. Dietrich, C. Ott., and A. Albu-Schaffer, “Coordination of thrusters, reaction wheels, and arm in orbital robots,” *Robotics and Autonomous Systems*, vol. 131, 2020.
- [15] A. M. Giordano, “Whole-Body Control of Orbital Robots,” Ph.D. dissertation, Technical University Munchen, 2020.
- [16] E. Papadopoulos and S. Dubowsky, “Coordinated manipulator/spacecraft motion control for space robotic systems,” in *Proceedings of the 1991 IEEE International Conference on Robotics and Automation*, 1991.
- [17] B. Siciliano, L. Sciavicco, L. Villani, and G. Oriolo, *Robotics Modelling, Planning and Control*. Springer, 2009.
- [18] D. Invernizzi, S. Panza, and M. Lovera, “Robust Tuning of Geometric Attitude Controllers for Multirotor Unmanned Aerial Vehicles,” *Journal of Guidance, Control, and Dynamics*, vol. 43, no. 7, pp. 1332–1343, 2020.
- [19] J. W. Burdick, “On the Inverse Kinematics of Redundant Manipulators: Characterization of the Self-Motion Manifolds,” in *Proceedings of the 4th International Conference on Advanced Robotics*, 1989.
- [20] C. R. Carignan, “Trajectory optimization for kinematically redundant arms,” *Journal of Robotic Systems*, vol. 8, no. 2, pp. 221–248, 1991.
- [21] B. Siciliano, “Kinematic control of redundant robot manipulators: A tutorial,” *Journal Intelligent and Robotic Systems*, vol. 3, pp. 201–212, 1990.
- [22] J. B. Rosen, “The Gradient Projection Method for Nonlinear Programming,” *Journal of the Society for Industrial and Applied Mathematics*, vol. 8, no. 1, pp. 181–217, 1960.
- [23] C. Ott, *Cartesian Impedance Control of Redundant and Flexible-Joint Robots*. Springer, 2008.
- [24] T. M. Inc., *Control System Toolbox User’s Guide*. The MathWorks, Inc., 2021.
- [25] F. Ankersen, “Guidance, Navigation, Control and Relative Dynamics for Spacecraft Proximity Maneuvers,” Ph.D. dissertation, Aalborg University, 2010.
- [26] W. Fehse, *Automated Rendezvous and Docking of Spacecraft*. Cambridge University Press, 2003, ISBN: 9780521824927.
- [27] X. Du, Y. He, L. Chen, and S. Gao, “Pose estimation of large non-cooperative spacecraft based on extended PnP model; Pose estimation of large non-cooperative spacecraft based on extended PnP model,” *2016 IEEE International Conference on Robotics and Biomimetics (ROBIO)*, 2016.
- [28] H. Mishra and P. Schmidt, “Motion and parameter estimation for the robotic capture of a non-cooperative space target considering egomotion uncertainty,” 2017.
- [29] P. Colmenarejo, J. Branco, *et al.*, “Methods and outcomes of the COMRADE project - Design of robust Combined control for robotic spacecraft and manipulator in servicing missions: comparison between Hinf and nonlinear Lyapunov-based approaches,” 2018.
- [30] R. Opromolla and A. Nocerino, “Uncooperative Spacecraft Relative Navigation With LIDAR-Based Unscented Kalman Filter,”
- [31] L. P. Cassinis *et al.*, “Evaluation of tightly- and loosely-coupled approaches in CNN-based pose estimation systems for uncooperative spacecraft,” *Acta Astronautica*, vol. 182, pp. 189–202, 2021.
- [32] J. D. Foley, M. A. Fischler, and R. C. Bolles, “Graphics and Image Processing Random Sample Consensus: A Paradigm for Model Fitting with Applications to Image Analysis and Automated Cartography,” 1981.

- [33] B. E. Tweddle and A. Saenz-Otero, "Relative Computer Vision-Based Navigation for Small Inspection Spacecraft," *Journal of Guidance, Control, and Dynamics*, vol. 38, no. 5, pp. 969–978, 2015.
- [34] S. Garrido-Jurado, R. Muñoz-Salinas, F. J. Madrid-Cuevas, and M. J. Marín-Jiménez, "Automatic generation and detection of highly reliable fiducial markers under occlusion," *Pattern Recognition*, vol. 47, no. 6, pp. 2280–2292, 2014.
- [35] H. P. Gavin, "The Levenberg-Marquardt algorithm for nonlinear least squares curve-fitting problems," 2020.
- [36] K. Klionovska and M. Burri, "Hardware-in-the-Loop Simulations with Umbra Conditions for Spacecraft Rendezvous with PMD Visual Sensors," *Sensors*, vol. 21, no. 4, 2021.
- [37] P. J. Besl and N. D. McKay, "A method for registration of 3-D shapes," *IEEE Transactions on Pattern Analysis and Machine Intelligence*, vol. 14, no. 2, pp. 239–256, 1992.
- [38] MATLAB, *Simscape Multibody 2020b*. Natick, Massachusetts: The MathWorks Inc., 2020.
- [39] H. N. Abramson, "Fluid Management in Microgravity," in *The dynamic Behavior of Liquids in moving Containers*, 2000.
- [40] N. Pavlis, S. Holmes, S. Kenyon, and J. Factor, "The development and evaluation of the Earth Gravitational Model 2008 (EGM2008)," *Journal of geophysical research: solid earth*, 2012.
- [41] P. Alken, E. Thébault, *et al.*, "International Geomagnetic Reference Field: the thirteenth generation," *Earth, Planets and Space*, vol. 73, no. 1, p. 49, 2021.
- [42] J. R. Wertz, "Modeling the Space Environment," in *Spacecraft Attitude Determination and Control*, 1987, pp. 113–149.
- [43] Government Publishing Office, *The Astronomical Almanac for the Year 2020*. 2020.
- [44] J. M. Picone, A. E. Hedin, D. P. Drob, and A. C. Aikin, "NRLMSISE-00 empirical model of the atmosphere: Statistical comparisons and scientific issues," *Journal of Geophysical Research: Space Physics*, vol. 107, no. A12, Dec. 2002.
- [45] M. List, S. Bremer, B. Rievers, and H. Selig, "Modelling of Solar Radiation Pressure Effects: Parameter Analysis for the MICROSCOPE Mission," *International Journal of Aerospace Engineering*, vol. List, p. 14, 2015.
- [46] K. Yoshida, R. Kurazamei, N. Sashida, and Y. Umetani, "Modeling of Collision Dynamics for Space Free-Floating Links with Extended Generalized Inertia Tensor," in *Proceedings of the 1992 IEEE International Conference on Robotics and Automation*, 1992.
- [47] —, "Modeling of Impact Dynamics and Impulse Minimization," in *Proceedings of the 1993 IEEE/RSJ International Conference on Intelligent Robots and Systems*, 1993.